Spectroscopic study of ^{20}Ne+p reactions using the JENSA gas-jet target to constrain the astrophysical ^{18}F(p,α)^{15}O rate

D. W. Bardayan, K. A. Chipps, S. Ahn, J. C. Blackmon, S. Carmichael, U. Greife, K. L. Jones, J. José, A. Kontos, R. L. Kozub, L. Linhardt, B. Manning, M. Matoš, P. D. O'Malley, S. Ota, S. D. Pain, W. A. Peters, S. T. Pittman, A. Sachs, K. T. Schmitt, M. S. Smith, and P. Thompson

Phys. Rev. C **96**, 055806 — Published 16 November 2017

DOI: 10.1103/PhysRevC.96.055806

Spectroscopic study of ^{20}Ne+p reactions using the JENSA gas-jet target to constrain the astrophysical ^{18}F$(p,\alpha)^{15}$O rate

D. W. Bardayan,[1,2] K. A. Chipps,[2,3,4] S. Ahn,[4] J. C. Blackmon,[5] S. Carmichael,[6] U. Greife,[3] K. L. Jones,[4] J. José,[7,8] A. Kontos,[9] R. L. Kozub,[10] L. Linhardt,[5] B. Manning,[11,12] M. Matoš,[2,4] P. D. O'Malley,[1] S. Ota,[11] S. D. Pain,[2] W. A. Peters,[2,4] S. T. Pittman,[2,4] A. Sachs,[4] K. T. Schmitt,[2,4,12] M. S. Smith,[2] and P. Thompson[4]

[1]*Physics Department, University of Notre Dame, Notre Dame, IN 46556, USA*
[2]*Physics Division, Oak Ridge National Laboratory, Oak Ridge, TN 37831, USA*
[3]*Physics Department, Colorado School of Mines, Golden, CO 80401, USA*
[4]*Department of Physics and Astronomy, University of Tennessee, Knoxville, TN 37996, USA*
[5]*Department of Physics and Astronomy, Louisiana State University, Baton Rouge, LA 70803, USA*
[6]*Department of Physics and Astronomy, Northwestern Univeristy, Evanston, IL 60208, USA*
[7]*Departament de Física, Universitat Politècnica de Catalunya, EEBE, E-08930 Barcelona, Spain*
[8]*Institut d'Estudis Espacials de Catalunya (IEEC), E-08034 Barcelona, Spain*
[9]*National Superconducting Cyclotron Laboratory, East Lansing, MI 48824, USA*
[10]*Department of Physics, Tennessee Technological University, Cookeville, TN 38505, USA*
[11]*Department of Physics and Astronomy, Rutgers University, Piscataway, NJ 08854, USA*
[12]*Physics Division, Los Alamos National Laboratory, Los Alamos, NM 87545, USA*

The Jet Experiments in Nuclear Structure and Astrophysics (JENSA) gas-jet target has been used to perform spectroscopic studies of ^{20}Ne+p reactions. Levels in ^{19}Ne were probed via the ^{20}Ne$(p,d)^{19}$Ne reaction to constrain the astrophysical rate of the ^{18}F$(p,\alpha)^{15}$O reaction. Additionally, the first spectroscopic study of the ^{20}Ne$(p,^3$He$)^{18}$F reaction was performed. Angular distribution data were used to determine or confirm the spins of several previously-observed levels, and the existence of a strong subthreshold ^{18}F$(p,\alpha)^{15}$O resonance was verified.

PACS numbers: 25.40.Hs, 26.30.Ca, 27.20.+n, 29.25.Pj

I. INTRODUCTION

The astrophysical rate of the ^{18}F$(p,\alpha)^{15}$O reaction determines, in part, the amount of potentially-observable ^{18}F that is ejected from novae. Observations of such ejecta would provide a rather direct constraint on nova models [1–3]. The rate of the ^{18}F$(p,\alpha)^{15}$O reaction is determined by the properties of ^{19}Ne levels near and above the proton threshold at 6.4100(5) MeV. Because of this importance, the ^{18}F$(p,\alpha)^{15}$O reaction has been studied with a variety of direct [4–8] and indirect measurements with both stable [9–12] and radioactive beams [13–16]. Additional guidance has come from compilations [17] and theoretical studies [18]. These studies have indicated that uncertainties in the rate may be large because of the uncertain interference between near-threshold resonances and broad higher-lying $\frac{1}{2}^+$ and $\frac{3}{2}^+$ resonances. These uncertainties have been exacerbated by the lack of spin assignments for the near-threshold [11] and subthreshold [15] levels.

II. EXPERIMENT

To further study the spins of these levels, a spectroscopic study of the ^{20}Ne$(p,d)^{19}$Ne reaction was performed at the Holifield Radioactive Ion Beam Facility (HRIBF) [19]. First results have been presented in Bardayan *et al.* [20]. In this follow-up manuscript, further experimental and analysis details are presented along with data from the ^{20}Ne$(p,^3$He$)^{18}$F reaction channel, which was measured simultaneously.

The JENSA [21] gas-jet target was used to create a localized (4 mm) and dense (4×10^{18} atoms/cm^2) ^{nat}Ne target ($\sim 90.5\%$ ^{20}Ne), which was bombarded with a 30-MeV proton beam (3 nA) from the HRIBF. The beam was tuned and focused to a spot size of 2-3 mm at an optically-aligned retractable scintillating phosphor ensuring spatial overlap with the JENSA gas jet. Reaction ejectiles were detected and identified using elements of the SIDAR Silicon Detector Array [22] configured in telescope mode with 65-μm-thick ΔE detectors being backed by 1000-μm-thick E detectors and covering laboratory angles between $18^\circ - 53^\circ$. A particle-identification spectrum from the experiment is plotted in Fig. 1. The various observed particle groups ($p,d,t,^3$He, and ^{4}He ions) were well separated using this energy-loss technique. The most intense group (10-20 kHz) arose from elastically-scattered protons, which were preferentially suppressed from the data acquisition by applying a hardware energy threshold to the ΔE detector signals. This reduced the trigger rate to ~ 4 kHz and the data acquisition deadtime to 15%, but the high rate still produced a small amount of pile-up pollution (e.g., the counts between the H and He groups) to the other particle groups as observed in the particle-identification plot. This generally resulted in a smoothly-varying background that could be subtracted in analysis. Data were taken in event mode for 15 hours and later replayed in software where small corrections to detector channel gain inhomogeneities could be applied. This was important since data from all detectors at the same angle were summed to maximize statis-

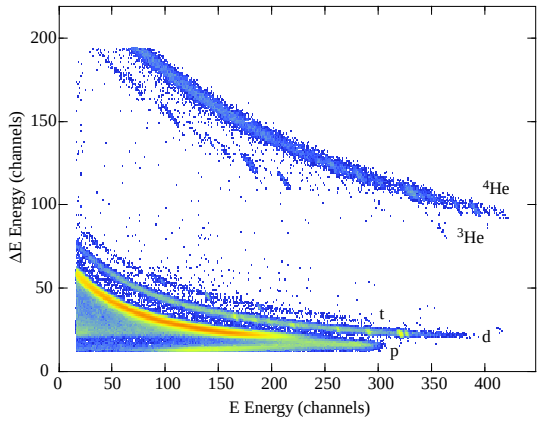

FIG. 1: (color online) A particle identification spectrum produced by plotting the energy loss in the ΔE 65-μm-thick detector on the vertical axis against the residual energy deposited in the 1000-μm-thick E detector on the horizontal axis.

tics in the excitation energy spectrum. Examples of the compiled energy spectra are plotted in Fig. 2 for the ^{20}Ne$(p,d)^{19}$Ne reaction as measured at three demonstrative angles.

III. ^{20}Ne$(p,d)^{19}$Ne ANALYSIS

An internal calibration was performed using the strongly-populated ^{19}Ne levels at 0, 2794.7(6), and 6742(7) keV. Using such an internal calibration helps minimize systematic uncertainties related to absolute energy and position calibrations. As shown in Bardayan *et al.* [20], there was excellent correspondence between the observed peaks in the spectrum and known levels in ^{19}Ne. The only observed peaks that did not correspond to known ^{19}Ne levels could be traced to (p,d) reactions on the ^{22}Ne atoms in the ^{nat}Ne target gas. The identification of the observed peaks was further verified from their kinematic shifts as a function of angle. An example for the observed ^{19}Ne level at E_x=6288 keV is shown in Fig. 3. The observed deuteron energies agree with the expected energies from reaction kinematics. The excitation energies measured in this work were reported in Ref. [20] and are repeated here in Table I for completeness.

A primary goal of the present work was to determine the spin of the subthreshold ^{18}F$(p,\alpha)^{15}$O resonance arising from the ^{19}Ne level at E_x=6288 keV. This state was populated strongly with an ℓ=0 transfer in a previous ^{18}F$(d,n)^{19}$Ne measurement and could give rise to significant interference effects in the ^{18}F$(p,\alpha)^{15}$O cross section if it has $J^\pi = \frac{3}{2}^+$ [15]. Unfortunately, the study by Adekola *et al.* could not distinguish angular distributions produced by populating $\frac{1}{2}^+$ or $\frac{3}{2}^+$ levels, and considerable uncertainty in the ^{18}F$(p,\alpha)^{15}$O reaction rate remained. This ambiguity, however, could be resolved by studying the level with the ^{20}Ne$(p,d)^{19}$Ne reaction where population of a $\frac{1}{2}^+$ or $\frac{3}{2}^+$ level would require an $\ell = 0$ or $\ell = 2$ transfer, respectively. The angular distributions of deuterons produced in such transfers would have significantly different shapes such that the two possibilities could be distinguished.

TABLE I: The ^{19}Ne excitation energies in keV from this work are compared with those from the most recent evaluation [23]. The states marked with an asterisk were used for the internal energy calibration. Only statistical uncertainties are quoted. There is an additional systematic uncertainty in the present results estimated to be ±3 keV.

present work	Compilation
2(2)	0*
255(2)	238.27(11) + 275.09(13)
1524(2)	1507.56(30) + 1536.0(4)
1604(3)	1615.6(5)
2792(3)	2794.7(6)*
4035(4)	4032.9(24)
4153(4)	4140(4)
4371(3)	4379.1(22)
4556(3)	4549(4)
5090(6)	5092(6)
5424(7)	5424(7)
5529(10)	5539(9)
6017(3)	6013(7)
6101(4)	6092(8)
6282(3)	6288(7)
6438(2)	6437(9)
6742(3)	6742(7)*
6865(3)	6861(7)
7067(2)	7067(9)

Angular distributions have been extracted for the strongly populated levels with an emphasis on obtaining the 6288-keV angular distribution. The angles and solid angles subtended by the detector strips were calculated from the known detector geometry. The consistency (Fig. 3) between the angular dependence of the observed deuteron energies and those calculated from kinematics provides further verification of the detector geometry. The angular distributions extracted (including population of the 6288-keV level) are plotted in Fig. 4 and listed in Table II. The data are plotted with arbitrary units since the beam current was not measured during the experiment. This does not jeopardize the analysis, however, since only the shape of the angular distribution is necessary to determine the transferred angular momentum. Cross section data are not reported at some angles if the peak of interest had too few statistics, was not resolved from a nearby peak, or was cut off by a discriminator threshold.

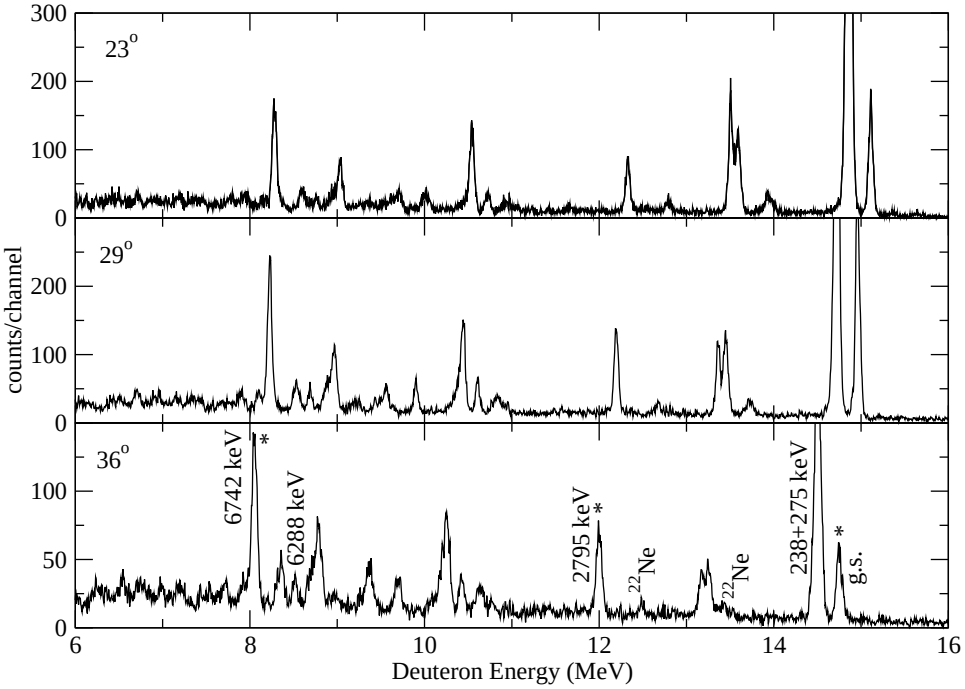

FIG. 2: The deuteron energy spectra observed from the ^{20}Ne$(p,d)^{19}$Ne reaction. The levels used for calibration are marked with an asterisk. Resolution of ∼70 keV was obtained, which was mostly a result of the kinematic shift of deuterons over the angles covered by the detectors.

TABLE II: The number of counts divided by the solid angle covered in the center of mass (i.e., angular distributions) extracted for the population of states in the ^{20}Ne$(p,d)^{19}$Ne reaction as a function of center-of-mass angle in degrees. The cross sections should be considered relative (to each other) values since the beam current was not measured.

g.s.		238+275 keV		1616 keV		2795 keV		5092 keV		6288 keV		6742 keV	
$\theta_{c.m.}$	$\frac{d\sigma}{d\Omega}$	$\theta_{c.m.}$	$\frac{d\sigma}{d\Omega}$	$\theta_{c.m.}$	$\frac{d\sigma}{d\Omega}$	$\theta_{c.m.}$	$\frac{d\sigma}{d\Omega}$	$\theta_{c.m.}$	$\frac{d\sigma}{d\Omega}$	$\theta_{c.m.}$	$\frac{d\sigma}{d\Omega}$	$\theta_{c.m.}$	$\frac{d\sigma}{d\Omega}$
23.0	15.4 ± 0.7	23.0	168.6 ± 1.9	23.1	28 ± 2	23.2	12.4 ± 0.8	23.5	3.8 ± 0.9	28.2	1.5 ± 0.3	23.8	22.9 ± 1.0
25.2	25.6 ± 0.7	25.2	168.6 ± 1.7	25.3	27.2 ± 0.9	25.4	13.1 ± 0.6	25.8	4.8 ± 0.5	30.5	1.3 ± 0.3	26.1	26.7 ± 0.8
27.4	41.9 ± 0.9	27.4	142.3 ± 1.5	27.5	19.6 ± 0.8	27.7	13.5 ± 0.5	28.0	4.9 ± 0.4	32.9	1.7 ± 0.3	28.3	25.4 ± 0.6
29.5	46.2 ± 0.9	29.6	113.6 ± 1.3	29.7	17.1 ± 0.7	29.9	13.1 ± 0.6	30.2	3.8 ± 0.3	35.3	1.5 ± 0.3	30.6	22.6 ± 0.6
31.8	45.0 ± 0.8	31.9	91.8 ± 1.1	32.0	12.0 ± 0.5	32.2	14.0 ± 0.5	32.6	3.8 ± 0.3	37.8	0.6 ± 0.3	33.0	21.0 ± 0.5
34.2	35.4 ± 1.0	34.3	74.4 ± 1.4	34.4	8.4 ± 1.0	34.6	13.0 ± 0.5	35.0	3.5 ± 0.3	40.4	1.3 ± 0.3	35.5	19.9 ± 0.5
36.6	24.2 ± 0.8	36.7	61.7 ± 1.3			37.0	13.4 ± 0.8	37.5	3.1 ± 0.5	42.9	1.0 ± 0.2	37.9	19.5 ± 0.6
39.1	14.9 ± 0.7	39.2	63.9 ± 1.2			39.6	13.4 ± 0.7	40.0	3.7 ± 0.4	45.5	1.0 ± 0.2	40.5	17.4 ± 0.5
41.6	8.9 ± 0.6	41.7	62.2 ± 1.1			42.1	13.1 ± 0.7	42.6	2.3 ± 0.3	48.0	0.7 ± 0.2	43.1	14.8 ± 0.4
46.6	6.0 ± 0.4	46.6	46.8 ± 0.9			47.1	9.9 ± 0.5	45.1	2.3 ± 0.3	50.7	0.8 ± 0.3	45.7	13.0 ± 0.4
49.2	5.3 ± 0.4	49.2	33.8 ± 0.8			49.7	9.3 ± 0.5	47.7	2.4 ± 0.2	53.2	0.6 ± 0.2	48.2	13.3 ± 0.4
51.7	3.7 ± 0.3	54.3	30.3 ± 0.8			52.2	9.5 ± 0.6	50.3	2.8 ± 0.3			50.9	13.0 ± 0.4
54.2	10.1 ± 0.6	56.8	29.2 ± 1.1			54.8	8.7 ± 0.6					53.4	12.7 ± 0.4
56.8	15.7 ± 0.9					57.4	5.2 ± 0.6					56.0	7.5 ± 0.7

The extracted angular distributions were compared to finite-range distorted-wave Born approximation (DWBA) calculations using the computer code TWOFNR18 [24]. Global optical model sets were used and found to provide a reasonable description of the angular distributions for populating levels with known spins. The optical model parameters used are given in table III. As can be seen in Fig. 4, the angular distribution populating the 6288-keV ^{19}Ne level agrees much better with the calculated $\ell = 0$ angular momentum transfer than for $\ell = 2$. This therefore indicates that the sub-threshold ^{18}F$(p,\alpha)^{15}$O resonance has $J^\pi = \frac{1}{2}^+$.

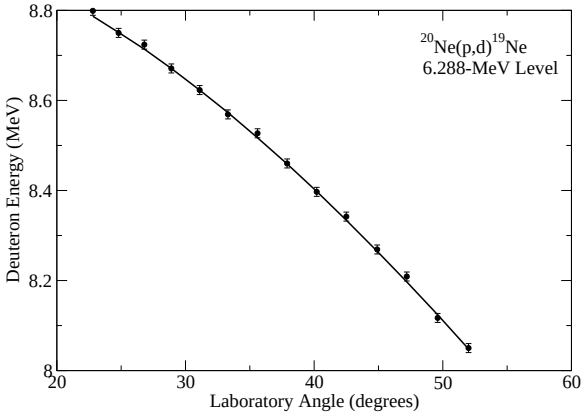

FIG. 3: Data points depicting the observed deuteron energies for population of the 6288-keV ^{19}Ne level. The line shows the expected energies as a function of angle from kinematics.

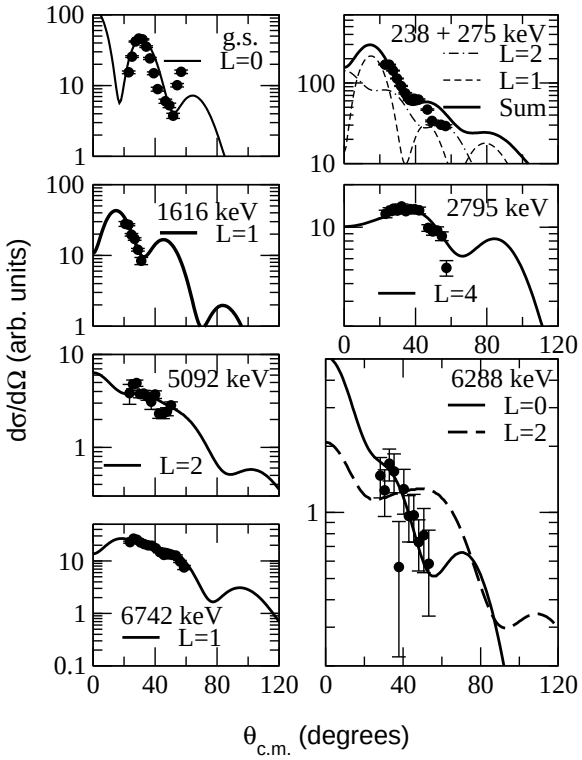

FIG. 4: Extracted angular distributions for the ^{20}Ne$(p,d)^{19}$Ne reaction from Ref. [20] and repeated here for completeness.

IV. ^{20}Ne$(p,^3$He$)^{18}$F ANALYSIS

While the focus of the experiment was to study the ^{20}Ne$(p,d)^{19}$Ne reaction, other reaction channels were also clearly present as seen in Fig. 1 and measured simultaneously. Of these other channels, the ^{3}He channel was the mostly likely to yield spectroscopic information since the excitation energy region ($E_x = 0-6$ MeV) populated by ejectiles identifiable in the telescopes is characterized by a level density resolvable within the energy resolution of the system ($\sim$ 60 keV). While there has been a single previous study of the ^{20}Ne$(p,^3$He$)^{18}$F reaction [28], a spectroscopic study of the levels populated in the reaction has not been previously reported.

TABLE III: Global optical model parameters used in the calculation of DWBA cross sections. The proton parameters were from Perey and Perey [25], the deuteron parameters were from Lohr and Haeberli [26], and the ^{3}He parameters were from Becchetti and Greenlees [27].

Parameter	p	d	^{3}He
V_r (MeV)	38.3	99.4	149.5
r_o (fm)	1.25	1.05	1.20
a_o (fm)	0.65	0.86	0.72
W_s (MeV)	13.5	30.6	0.00
r_I (fm)	1.25	1.43	1.40
a_I (fm)	0.47	0.59	0.88
W_V (MeV)	0.00	0.00	37.1
V_{SO} (MeV)	7.50	3.50	2.50
r_{SO} (fm)	1.25	0.75	1.20
a_{SO} (fm)	0.47	0.50	0.72

Similar to the ^{20}Ne$(p,d)^{19}$Ne data, events associated with ^{3}He ejectiles were selected in software for analysis. The energies from the ΔE and E detectors were summed and carefully gain matched between telescopes. The total energy spectra were then projected, and an example from $\theta_{lab} = 29^\circ$ is plotted in Fig. 5. As seen in Fig. 5, there was once again excellent agreement between the observed peaks and the known ^{18}F levels. An internal calibration of the data was performed using the well-separated and known levels at E_x =0, 1700.8(2), and 3358(1) keV. It was assumed that the calibration was linear since there was a lack of sufficient information to attempt a higher-order calibration. The energy levels extracted from this work are compared with compilation values in Table IV. Small differences are observed between the extracted and known energies, and thus a systematic uncertainty of 5 keV is estimated for the present data set.

Angular distributions have been extracted for the isolated lower-lying ^{18}F levels. Analysis of other levels was problematic due to the existence of mutliple doublets resulting in mostly featureless angular distributions. The exceptions are shown in Fig. 6 where the angular distribution are plotted with arbitrary units. The distributions were compared to TWOFNR18 calculations using global optical model parameters tabulated in Table III. The optical model parameters from Perey and Perey [25] were used for the initial state and Bechetti and Greenlees [27] for the exit channel. Reasonable agreement was observed between the calculated angular distributions and the observed ones assuming the lowest angular momentum transfer was dominant for a given spin. The results were consistent with known spin-parity assignments for the observed levels. The extracted relative cross sections

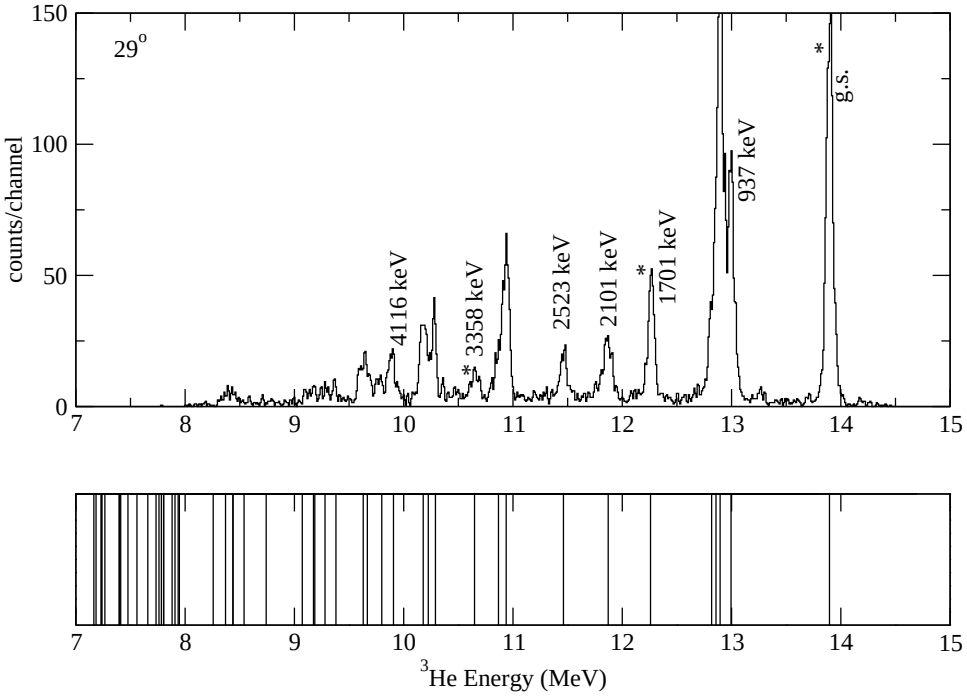

FIG. 5: The top panel shows the observed ^{3}He energy spectrum at 29° while the bottom panel shows the expected energies for the population of known levels in the ^{20}Ne(p,^{3}He)^{18}F reaction at the same angle and a bombarding energy of 30 MeV. Peaks labeled with asterisks were used for the internal energy calibration.

TABLE IV: The ^{18}F excitation energies in keV from this work are compared with those from the most recent evaluation [23]. The states marked with an asterisk were used for the internal energy calibration. Only statistical uncertainties are quoted. There is an additional systematic uncertainty in the present results estimated to be ±5keV.

Present work	Compilation	J^π
0(2)*	0.0	1^+
942(7)	937.20(6)	3^+
1043(2)	1041.55(8)	0^+
1085(6)	1080.54(12)	0^-
	1121.36(15)	5^+
1692(2)*	1700.81(18)	1^+
2092(4)	2100.61(10)	2^-
2515(5)	2523.35(18)	2^+
3068(3)	3061.84(18)	2^+
	3133.87(15)	1^-
3358(3)*	3358.2(10)	3^+
3734(11)	3724.19(22)	1^+
	3791.49(22)	2^+
3831(5)	3839.17(22)	2^+

are given in Table V.

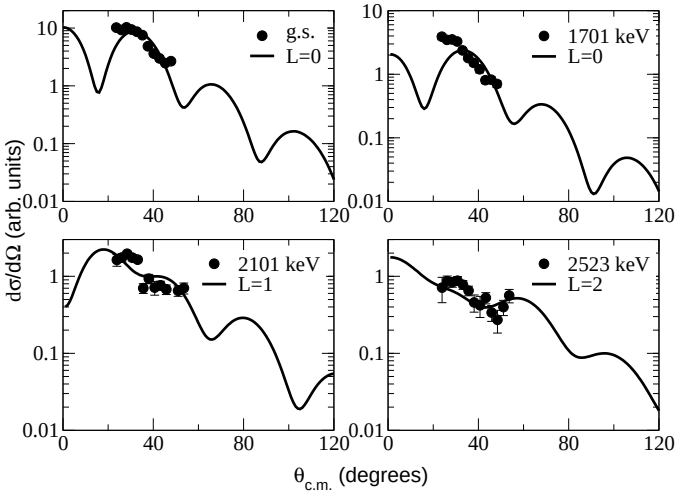

FIG. 6: Extracted angular distributions for the ^{20}Ne(p,^{3}He)^{18}F reaction. The distributions are compared to DWBA calculations using global optical model parameter sets.

V. ASTROPHYSICAL IMPLICATIONS

The astrophysical implications of the current measurement were discussed in Ref. [20]. In summary, the dominant uncertainty in the astrophysical ^{18}F$(p,\alpha)^{15}$O rate was the result of uncertain interference between sub- and

TABLE V: The number of counts divided by the solid angle covered in the center of mass (i.e., angular distributions) extracted for the population of states in the ^{20}Ne(p,^{3}He)^{18}F reaction as a function of center-of-mass angle in degrees. The cross sections should be considered relative (to each other) values since the beam current was not measured.

	g.s.		1701 keV		2101 keV		2523 keV
$\theta_{c.m.}$	$\frac{d\sigma}{d\Omega}$	$\theta_{c.m.}$	$\frac{d\sigma}{d\Omega}$	$\theta_{c.m.}$	$\frac{d\sigma}{d\Omega}$	$\theta_{c.m.}$	$\frac{d\sigma}{d\Omega}$
23.6	10.2 ± 0.6	23.8	3.9 ± 0.4	23.9	1.6 ± 0.3	23.9	0.7 ± 0.3
25.9	9.3 ± 0.4	26.1	3.5 ± 0.3	26.1	1.8 ± 0.2	26.2	0.87 ± 0.14
28.1	10.3 ± 0.3	28.4	3.5 ± 0.2	28.4	1.96 ± 0.16	28.5	0.84 ± 0.12
30.4	9.4 ± 0.3	30.6	3.28 ± 0.18	30.7	1.75 ± 0.16	30.8	0.88 ± 0.12
32.7	8.6 ± 0.3	33.0	2.37 ± 0.16	33.1	1.65 ± 0.14	33.2	0.78 ± 0.10
35.2	7.5 ± 0.2	35.5	1.80 ± 0.14	35.6	0.70 ± 0.10	35.6	0.65 ± 0.09
37.6	4.8 ± 0.2	38.0	1.51 ± 0.15	38.0	0.93 ± 0.13	38.1	0.46 ± 0.12
40.2	3.6 ± 0.2	40.5	1.20 ± 0.15	40.6	0.71 ± 0.15	40.7	0.42 ± 0.13
42.8	2.99 ± 0.15	43.1	0.81 ± 0.09	43.2	0.76 ± 0.10	43.3	0.53 ± 0.09
45.3	2.48 ± 0.14	45.7	0.80 ± 0.10	45.8	0.68 ± 0.10	45.9	0.34 ± 0.08
47.8	2.67 ± 0.13	48.2	0.70 ± 0.09	51.0	0.65 ± 0.10	48.4	0.27 ± 0.09
50.5	2.75 ± 0.12			53.5	0.70 ± 0.11		

near-threshold resonances and higher-lying broad s-wave resonances. There were several possibilities for the signs of this interference as a function of energy depending on the spins of the near-threshold resonances. Constraining the spin of the ^{19}Ne level at 6286(3) keV to be $\frac{1}{2}^+$ significantly reduced the number of possibilities resulting in a reduction in the astrophysical rate band width by as much as a factor of 4 in the temperature range 0.1-0.4 GK. The current uncertainty is less than a factor of 4 in the nova temperature range. Parameterizations of the low and high limits of the rate band were calculated [29] in the form

$$N_A < \sigma v >= \exp[a_1 + \sum_{i=2}^{6} a_i T^{2i/3-7/3} + a_7 \ln T] \quad (1)$$

where the reaction rate is given in cm^3/mole/s and the temperature, T, is in GK with coefficients listed in Table VI.

The impact of the uncertainties on ^{18}F production has been explored through a representative series of hydrodynamic nova simulations performed with the spherically symmetric, implicit, Langrangian code SHIVA [3, 30]. SHIVA simulates the evolution of nova outbursts from the onset of accretion to the explosion and ejection of nova material. The hydrodynamic code is coupled directly to the nuclear reaction network ensuring consistency between changes in the reaction network and the resulting energetics. Simulations utilized a 1.25 M$_\odot$ ONe white dwarf, accreting solar material (with a 50% premixing with material from the outermost ONe substrate) at a rate of 2×10^{-10} M$_\odot$ yr^{-1}. The final ^{18}F yields were compared one hour after the peak temperature (0.25 GK) was reached. It was found that the range of ejected ^{18}F mass has been reduced by factor of 1.92 owing to the reduction in uncertainty in the ^{18}F$(p,\alpha)^{15}$O rate. The results from the previously-reported "post-processing" approach [20] agree well with the present results from a fully-coupled set of hydrodynamics calculations.

VI. CONCLUSIONS AND ACKNOWLEDGMENTS

The JENSA gas-jet target has enabled a new class of experiments utilizing transfer reactions with gaseous targets and radioactive beams. The results of the first transfer reaction measurement using JENSA are reported here in further detail and expanding upon the initial report published as Ref. [20]. Energetic proton beams bombarded a natural Ne gas-jet target and reaction ejectiles probed the structure of a number of nuclei.

^{19}Ne was studied via the ^{20}Ne$(p,d)^{19}$Ne reaction in order to constrain the spin of a strong subthreshold ^{18}F$(p,\alpha)^{15}$O resonance. This resonance was found to have significant single-particle strength in previous ^{18}F$(d,n)^{19}$Ne measurements, but its contribution was uncertain, in part, because of its uncertain spin. The results from this study constrain its spin and parity to be $\frac{1}{2}^+$, and the uncertainty in the ^{18}F$(p,\alpha)^{15}$O rate is reduced by up to a factor of 4 in the nova temperature range. Nucleosynthesis calculations indicate that the uncertainty in ejected ^{18}F is reduced by roughly a factor of 2 owing to this result.

The structure of ^{18}F was studied simultaneously by detecting ejectiles from the ^{20}Ne(p,^{3}He)^{18}F reaction. Eleven ^{18}F levels were observed with energies agreeing with previous compilation values. The angular distributions were extracted for the low-lying isolated levels and agree with expectations for the known spins.

While this study has clarified ^{18}F$(p,\alpha)^{15}$O rate calculations, further improvements could come from a better determination of the strength of the 332-keV resonance (6742-keV level), measurements of the ^{18}F$(p,\alpha)^{15}$O cross

rate	a_1	a_2	a_3	a_4	a_5	a_6	a_7
low	0.125497×10^4	-0.147438×10^1	0.255995×10^3	-0.192537×10^4	0.664574×10^3	-0.255348×10^3	0.420723×10^3
high	0.981567×10^3	-0.130737×10^1	0.216525×10^3	-0.148303×10^4	0.429081×10^3	-0.135502×10^3	0.345346×10^3

TABLE VI: The coefficients, a_i, used to parameterize the ^{18}F$(p,\alpha)^{15}$O rate via a fit of Equation 1 to the calculated rate. The two sets of parameters are for low and high limits of the rate band.

section off-resonance to constrain the sign of the interference, observation of a predicted broad $\frac{1}{2}^+$ level [18] expected above $E_{c.m.} = 1$ MeV, or further clarification of the states near threshold in ^{19}Ne. The latter could come from γ-ray studies of ^{19}Ne [31].

This work was supported in part by the U.S. Department of Energy under Contract Nos. DE-FG02-10ER41704 and DE-FG02-93ER40789 (CSM), DE-FG52-08NA28552 (Rutgers), DE-FG02-96ER40983 (UTK), DE-FG02-96ER40955 (TTU), DE-AC05-00OR22725 (ORNL), and the National Science Foundation under Contract Nos. PHY-1419765 (Notre Dame) and PHY-0822648 (JINA). JJ acknowledges partial support by the Spanish MINECO grant AYA201459084P, and by the AGAUR/Generalitat de Catalunya grant SGR0038/2014.

[1] M. Hernanz, J. José, A. Coc, J. Gomez-Gomar, J. Isern, Astrophys. J. Lett. **526**, L97 (1999).
[2] M. Hernanz, in Classical Novae, M. F. Bode and A. Evans (editors), 2nd Ed., Cambridge Univ. Press, Cambridge, UK, 2008, pp 252-284.
[3] J. José,"Stellar explosions: hydrodynamics and nucleosynthesis", CRC/Taylor and Francis (2015).
[4] R. Coszach *et al.*, Phys. Lett. B **353**, 184 (1995).
[5] D. W. Bardayan *et al.*, Phys. Rev. C **63**, 065802 (2001).
[6] D. W. Bardayan *et al.*, Phys. Rev. Lett. **89**, 262501 (2002).
[7] C. E. Beer *et al.*, Phys. Rev. C **83**, 042801(R) (2011).
[8] D. J. Mountford *et al.*, Phys. Rev. C **85**, 022801(R) (2012).
[9] S. Utku *et al.*, Phys. Rev. C **57**, 2731 (1998).
[10] D. W. Visser *et al.*, Phys. Rev. C **69**, 048801 (2004).
[11] A. M. Laird *et al.*, Phys. Rev. Lett. **110**, 032502 (2013).
[12] A. Parikh *et al.*, Phys. Rev. C **92**, 055806 (2015).
[13] N. de Séréville *et al.*, Phys.Rev. C **67**, 052801 (2003).
[14] R. L. Kozub *et al.*, Phys. Rev. C **71**, 032801(R) (2005).
[15] A. S. Adekola *et al.*, Phys. Rev. C **83**, 052801(R) (2011).
[16] S. Cherubini *et al.*, Phys. Rev. C **92**, 015805 (2015).
[17] C. D. Nesaraja *et al.*, Phys. Rev. C **75**, 055809 (2007).
[18] M. Dufour and P. Descouvemont, Nucl. Phys. A **785**, 381 (2007).
[19] J. R. Beene *et al.*, J. Phys. G: Nucl. Part. Phys. **38**, 024002 (2011).
[20] D. W. Bardayan *et al.*, Phys. Lett. B **751**, 311 (2015).
[21] K. A. Chipps *et al.*, Nucl. Instrum. Meth. Phys. Res. A **763**, 553 (2014).
[22] D. W. Bardayan *et al.*, Phys. Rev. C **63**, 065802 (2001).
[23] D. R. Tilley, H. R. Weller, C. M. Cheves, R. M. Chasteler, Nucl. Phys. A **595**, 1 (1995).
[24] J. A. Tostevin, University of Surrey version of the code TWOFNR (of M. Toyama, M. Igarashi, and N. Kishida) and code FRONT (private communication).
[25] C. M. Perey and F. G. Perey, At. Data and Nucl. Data Tables **17**, 1 (1976).
[26] J. M. Lohr, W. Haeberli, Nucl. Phys. A **381**, 232 (1974).
[27] F. D. Becchetti, Jr. and G. W. Greenlees, Phys. Rev. **182**, 1190 (1969).
[28] J. C. Hardy, H. Brunnader, J. Cerny, J. Janecke, Phys. Rev. **183**, 854 (1969).
[29] http://nucastrodata.org
[30] J. José and M. Hernanz, Astrophys. J. **494**, 680 (1998).
[31] M. Hall *et al.*, Bull. Amer. Phys. Soc. **61**, 29 (2017).